ACCEPTED VERSION

Stella A. Child, Kate L. Flint, John B. Bruning, Stephen G. Bell
The characterisation of two members of the cytochrome P450 CYP150 family: CYP150A5 and CYP150A6 from Mycobacterium marinum
Biochimica et Biophysica Acta - General Subjects, 2019; 1863(5):925-934

Final publication at http://dx.doi.org/10.1016/j.bbagen.2019.02.016

The characterisation of two members of the cytochrome P450 CYP150 family: CYP150A5 and CYP150A6 from *Mycobacterium marinum*

Stella A. Child[1], Kate L. Flint[1], John B. Bruning[2], and Stephen G. Bell[1*]

[1]Department of Chemistry, University of Adelaide, SA 5005, Australia

[2]School of Biological Sciences, University of Adelaide, SA 5005, Australia

* To whom correspondence should be addressed.

Stephen G. Bell (stephen.bell@adelaide.edu.au)

Highlights

- Two *Mycobacterium marinum* cytochrome P450s of the CYP150A subfamily were characterised
- CYP150A5 binds a broad range of terpenoids and selectively oxidised β-ionol
- CYP150A6 binds a narrower range of substrates and was structurally characterised to 1.5 Å
- Members of the CYP150A subfamily were discovered across many bacteria, including in pathogens
- Azole inhibitors that bind with different affinities to CYP150A5 and CYP150A6 were identified

Abstract

Background

Actinobacteria, including the *Mycobacteria*, have a large component of cytochrome P450 family monooxygenases. This includes *Mycobacterium tuberculosis*, *M. ulcerans* and *M. marinum*, and the soil-dwelling *M. vanbaalenii*. These enzymes support hydroxylation of C–H bonds and have important roles in natural product biosynthesis.

Methods

Two members of the bacterial CYP150 family, CYP150A5 and CYP150A6 from *M. marinum*, were produced, purified and characterised. The substrate ranges of both enzymes were analysed and the monooxygenase activity of CYP150A5 was reconstituted using a physiological electron transfer partner system. CYP150A6 was structurally characterised by X-ray crystallography.

Results

CYP150A5 was shown to bind various norisoprenoids and terpenoid. It could regioselectively hydroxylate β-ionol. The X-ray crystal structure of substrate-free CYP150A6 was solved to 1.5 Å. This displayed an open conformation with short F and G helices, an unresolved F-G loop and exposed active site pocket. The active site residues could be identified and important variations were found among the CYP150A enzymes. Haem-binding azole inhibitors were identified for both enzymes.

Conclusions

Substrates were identified for CYP150A5. The structure of CYP150A6 will facilitate the identification of physiological substrates and the design of better inhibitors for members of this P450 family. Based on the observed differences in substrate preference and sequence variations among the active site residues, their roles are predicted to be different.

General Significance

Multiple CYP150 family members were found in many bacteria and are prevalent in the *Mycobacteria* including several human pathogens. Inhibition and structural data are reported here for these enzymes for the first time.

Keywords

Enzymology; electron transfer; biocatalysis; cytochrome P450; *Mycobacterium*; X-ray crystallography

Graphical abstract

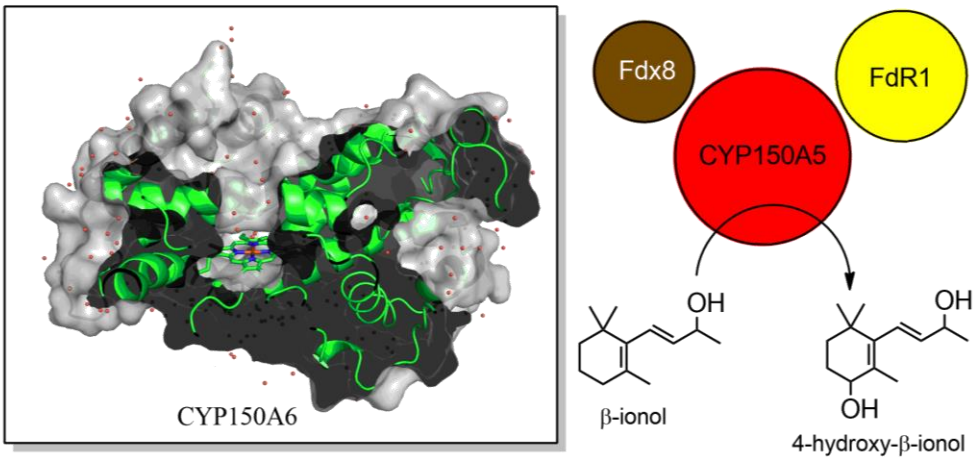

Abbreviations

2xYT, 2 x concentration yeast extract tryptophan broth; CYP or P450, Cytochrome P450 enzyme; DTT, dithiothreitol; EMM, *Esherichia coli* minimal media; FAD, flavin adenosine dinucleotide; FdR, ferredoxin reductase; Fdx, ferredoxin; GC-MS or MS, gas-chromatography mass spectrometry or mass spectrometry; IPTG, Isopropyl β-D-1-thiogalactopyranoside; LB, Lysogeny broth (also known as Luria or Lennox Broth), NAD(P)H reduced nicotinamide adenine dinucleotide (phosphate); PDB, Protein Data Bank; PDR, phthalate dioxygenase reductase; RT, retention time; SOC, Super Optimal broth with Catabolite repression.

1. Introduction

Cytochrome P450s (CYP or P450) are a family of haem monooxygenase enzymes. They act with a conserved mechanism to selectively insert an oxygen atom from molecular dioxygen into a carbon-hydrogen (C-H) bond of the substrate, forming an alcohol product [1]. Various CYP enzymes have also been found to catalyse other oxidation reactions, such as epoxidation, sulfoxidation, decarboxylation, hydrogenation, and carbon-carbon bond formation [2]. The catalytic cycle of the enzymes requires the transfer of electrons, ultimately derived from NADH or NADPH, to the haem via electron transfer proteins. Bacterial CYPs most frequently utilise a two component electron transfer system, comprised of an iron-sulfur ferredoxin and a FAD-containing ferredoxin reductase, which is termed a Class 1 system [3]. In a given genome, the number of genes tends to decrease in the order CYP > ferredoxin > ferredoxin reductase [4, 5]. The reconstruction of the native electron transfer chain for a given CYP enzyme is often required for optimal activity, as individual CYPs are often highly selective for a preferred ferredoxin [6, 7].

In humans, CYP enzymes are responsible for a large proportion of drug interactions but they are also widely found across plants, bacteria and fungi, performing both anabolic and catabolic roles [8, 9]. Due to their diversity, CYP enzymes are categorised into families, given a number, and sub-families, given a letter code, based on sequence similarities [10]. Members of the same family share >40% sequence identity, while sub-family members share >55%. Above 80% identity is sufficient for two enzymes to share a name. Bacterial CYPs have generally been investigated either as inhibition targets in pathogenic species, or as biocatalysts, as they frequently catalyse the formation of synthetically valuable compounds [9]. Functionalisation of C-H bonds is particularly difficult to achieve by chemical methods, often requiring harsh conditions and resulting in poor selectivity. In contrast, CYPs often

display very high selectivity of oxidation, and regio- and stereo- selectivity in product formation is widespread [11].

Mycobacterium tuberculosis, the pathogen responsible for human tuberculosis, has been the target of ongoing drug development efforts as increasing levels of resistance to first and second-line anti-tuberculosis drugs is seen globally [12]. There are 20 CYP enzyme encoding genes in *Mycobacterium tuberculosis*, several of which have been found to be essential for cell function or infectivity in the pathogen [13-15]. One of these, CYP121A1, which forms a carbon-carbon bond in the cyclic dipetide cyclo(l-Tyr-l-Tyr) has been subject to targeted inhibitor design [16-18]. Another, CYP128A1 has been implicated in virulence via the mediation of the metabolite sulfomenaquinone [19]. CYP125A1 and CYP142A1 are together necessary for *M. tuberculosis* cholesterol breakdown [20, 21]. In many other *Mycobacterium* species, the number of *cyp* genes is higher [22, 23]. The human pathogen *Mycobacterium ulcerans*, which causes the Buruli ulcer common in tropical areas of West Africa and Australia, has 24 while *Mycobacterium marinum*, a marine pathogen capable of opportunistic infection of humans, has 47 *cyp* genes [24, 25]. The lower number of CYPs in *M. ulcerans* and *M. tuberculosis* is thought to be caused by reductive evolution as they specialised towards pathogenicity [22-24]. *M. marinum*, in contrast to the two human pathogens, retains its ability to survive outside the host and is hypothesised to resemble the most recent common ancestor of *M. tuberculosis* and *M. ulcerans*, with which it shares a high degree of sequence identity (97% and 85%, respectively) [25]. Study of the CYP complement of *M. marinum* offers the understanding of the role and function of the additional CYPs, and hence the altered metabolism of the more pathogenic strains [26]. In addition, the CYPome of *M. marinum* is accompanied by a greater number of ferredoxins, with 12 single cluster containing species being associated with CYP enzymes in the genome [27]. Only three of these are retained in *M. tuberculosis*, while *M. ulcerans* retains seven.

M. marinum M contains two members of the CYP150 family, CYP150A5 and CYP150A6, which are the fifth and sixth members of the same sub-family. An analogue of CYP150A6 is present in *M. ulcerans* Agy99, but neither enzyme is conserved in *M. tuberculosis*. Other members of the CYP150 family have been identified in *Mycobacteria* including in *M. vanbaalenii* PYR-1 (CYP150A7). This enzyme has been characterised as having the potential to oxidise polycyclic aromatic hydrocarbons and is therefore of interest for its potential application in environmental remediation [28]. The CYP150A5 gene is beside a ferredoxin gene in the genome, and we have previously reported the enzyme is able to hydroxylate the fragrance compound β-ionone when coupled with a native electron transfer chain [27]. Here we report the biochemical and structural characterisation of the two enzymes CYP150A5 and CYP150A6 to gain insight into their function in the bacterial kingdom.

2. Experimental

2.1 General

All organic substrates, derivatisation agents and other general reagents, except where otherwise noted, were purchased from Sigma-Aldrich, Alfa-Aesar, VWR International or Tokyo Chemical Industry. Antibiotics, detergents, DTT and IPTG were from Astral Scientific. The media for cell growth and maintenance (LB, 2xYT, SOC, EMM and trace elements) were prepared as reported previously [26, 29]. Antibiotics were added to the working concentrations listed here; ampicillin, 100 μg mL^{-1} and kanamycin, 30 μg mL^{-1}.

UV-Visible spectra were recorded on a Varian Cary 5000 at 30 ± 0.5 °C. GC-MS analysis was performed using a Shimadzu GC-17A equipped with a QP5050A MS detector and DB-5 MS fused silica column (30 m x 0.25 mm, 0.25 μm) or a Shimadzu GC-2010 equipped with a QP2010S GC-MS detector, AOC-20i autoinjector, AOC-20s autosampler and DB-5 MS fused silica column (30 m x 0.25 mm, 0.25 μm). On both instruments, the injector was held at 250 °C and the interface at 280 °C. Column flow was set at 1.5 mL min^{-1} and the split ratio was 24. For norisoprenoid analysis, the initial oven temperature was 120 °C (held for 3 min), before increasing to 220 °C at 10 °C min^{-1}, where it was maintained for 7 min.

2.2 CYP150A6 production and purification

CYP150A6 was purified according to the same method as reported previously for CYP150A5, using two ion-exchange steps [27]. Before each use, the stored protein samples were buffer exchanged into 50 mM Tris (pH 7.4) using a PD-10 desalting column (5 mL, GE Healthcare) to remove glycerol. The CYP150A5 concentration was determined using ε_{419} = 111 ± 4 mM^{-1} cm^{-1} [27]. The extinction coefficient of CYP150A6 was determined by the CO binding assay initially developed by Omura and Sato [30] which was performed as described previously [26].

2.3 Spin-state shift assays and dissociation constant determination

The CYP enzymes were diluted to ~1 µM using 50 mM Tris (pH 7.4) buffer and the UV/Vis spectrum was recorded between 600 and 250 nm, while held at 30 °C. Aliquots (1 to 5 µL) of substrate stock solutions (50 mM or 100 mM, DMSO or EtOH) were added. The spectra were recorded until the shift reached a stable point. The ratio of high spin to low spin CYP (390 nm peak to 420 nm peak) was estimated to ± 5% by comparison to the $P450_{cam}$–camphor bound substrate spectra [26].

To measure the binding affinity, the CYP enzymes were diluted to ~2 µM in a volume of 2.5 mL in 50 mM Tris (pH 7.4) buffer and used to baseline the spectrophotometer. Varying aliquots (1 to 3 µL) of substrate stock solutions of increasing concentrations (1 mM, 10 mM or 100 mM) were added via a Hamilton syringe and mixed. The difference spectrum was recorded between 300 nm and 600 nm. Further aliquots of substrate were added until no change in the peak-to-trough ratio at ~420 nm and ~390 nm (for a Type I spectrum) or ~410 and ~430 nm (for a Type II spectrum) was observed. The difference in absorbance versus substrate concentration was fitted to the hyperbolic function (Equation 1):

$$\Delta A = \frac{\Delta A_{max} \times [S]}{K_d + [S]}$$

where K_d is the dissociation constant, [*S*] is the substrate concentration, ΔA the peak-to-trough ratio, and ΔA_{max} the maximum peak-to-trough absorbance. Where a particular substrate exhibited tight binding (K_d equalling less than five times the concentration of the enzyme), the data were instead fitted to the tight-binding quadratic equation:

$$\Delta A = \Delta A \times \frac{[E] + [S] + K_d - \sqrt{([E] + [S] + K_d)^2 - 4[E][S]}}{2[E]}$$

where K_d is the dissociation constant, [*S*] is the substrate concentration, ΔA the peak-to-trough ratio, ΔA_{max} the maximum peak-to-trough absorbance and [*E*] is the enzyme concentration [31].

2.4 Whole-cell oxidation turnovers

Whole-cell turnovers with CYP150A5 were performed as per the method previously reported [26]. Briefly, a pRSFDuet vector containing the genes of the CYP and Fdx8, and a pETDuet vector containing the Fdx8 and FdR1 genes used for expression in *E. coli* BL21(DE3) cells. These were grown in LB with the appropriate antibiotics and trace elements (3 mL L^{-1}) at 37 °C. Alternative pETDuet vectors were used containing genes for the electron transfer partners listed in Table S1. Once the cells reached late log phase, the temperature was reduced to 18 °C. Benzyl alcohol (0.02% v/v), ethanol (2% v/v) were added and protein expression was induced after a further 30 min with IPTG (0.1 mM). After 16 h, the cells were resuspended in *E. coli* minimal media (EMM) and the substrates added to a final concentration of 1 mM and shaken for a further 24 h. Aliquots of these growths (including cells) were extracted into ethyl acetate, and analysed by GC-MS.

2.5 Phylogenetic analysis

Sequences were obtained either from the National Centre for Biotechnology Information (NCBI) database or from the Dr Nelson P450 homepage for bacterial P450s [32]. Sequence alignments were performed using ClustalW [33]. The evolutionary history was inferred by using the Maximum Likelihood method based on the Jones-Taylor-Thornton (JTT) matrix-based model [34]. Initial trees for the heuristic search were obtained automatically by applying Neighbor-Join and BioNJ algorithms to a matrix of pairwise distances estimated using a JTT model, and then selecting the topology with superior log likelihood value. The tree is drawn to scale, with branch lengths measured in the number of substitutions per site. All positions containing gaps and missing data were eliminated. Evolutionary analyses were conducted in MEGA6 [35].

2.6 Crystallography

CYP150A5 and CYP150A6 underwent a further purification step by size exclusion (Enrich SEC Column, 650 x 10 x 300 mm, 1 mL min^{-1}) before concentration to ~30 mg mL^{-1} in 50 mM Tris (pH 7.4). Commercially available screening conditions (Hampton Research) were used for initial screening in 96 well sitting drop trays, using 1 µL of both protein and reservoir solution. Crystal conditions were then refined using the hanging drop vapour diffusion method, again using both 1 µL of protein and reservoir solution with a 500 µL reservoir. Diffraction quality crystals of CYP150A6 were obtained after 2 weeks at 16 °C from the condition containing 0.2 M ammonium phosphate, 20% w/v polyethylene glycol 3,350, pH 4.7. The crystals were harvested using a Micromount (MiTeGen) and cryo-protected by immersion in Parabar 10312 (Paratone-N, Hampton Research) before flash cooling in liquid N_2. Data were collected by X-ray diffraction at the Australian Synchrotron MX1 beamline (360 exposures using 1° oscillations at a wavelength of 0.9357 Å) at 100 K [36]. The data were processed into the space group $P3_121$ using iMosflm [37], followed by truncation and addition of R_{free} flags using Aimless [38], as part of the CCP4 package [39]. Molecular replacement phasing was carried out using the MrBump pipeline [40], also part of CCP4, comprising PhaserMR [41] and one round of Buccaneer [42] model building and refinement. The search model used was PDB:3EJD [43], prepared for molecular replacement by MOLREP [44]. The model was rebuilt using Coot [45] based on initial electron density maps and refined using phenix.refine [46] over several iterations. The structure was deposited in the Protein data bank (PDB: 6DCB) and the data collection and refinement statistics are presented in Table 1.

Table 1: Crystal data collection and refinement statistics for CYP150A6 from *M. marinum* (PDB: 6DCB)

Data collection statistics[a]	
Wavelength	0.95370
Unit cell	a = 80.57 b = 80.57 c = 134.76
	α = 90 β = 90 γ = 120
Space group	$P3_121$
Mol. in asym. unit	1
Resolution	48.47 – 1.55 (1.57 – 1.55)[b]
Unique reflections	74838 (3655)
Completeness	100.0 (100.0)
Redundancy	22.0 (20.7)
(I)/[σ(I)]	11.7 (0.8)
R_{merge} (all I+ and I-)	0.26 (4.72)
R_{pim} (all I+ and I-)	0.057 (1.056)
CC(1/2)	0.99 (0.36)
R_{work}	0.223 (0.342)
R_{free}	0.247 (0.349)
% solvent	53.46
Residues modelled	406
RMS deviation from restraint values	
Bond lengths	0.004
Bond angles	0.80
Ramachandran analysis	
Most favoured	97.8
Additionally allowed	2.2
Disallowed	0

[a] Data collected from one crystal

[b] Values in parenthesis are for highest resolution shell.

3. Results/Discussion

3.1 Phylogenetic analysis

The CYP150 family has only one named subfamily at present (according to the Cytochrome P450 Homepage maintained by Dr Nelson of the University of Tennessee [32]). There are 15 members of the subfamily that have been assigned CYP names so far, all of which are found in either *Mycobacterium* or *Frankia* species. CYP150A5 and CYP150A6 are both found in *M. marinum* M, with a CYP150A6 species also found in *M. ulcerans* Agy99 (98% sequence identity). Other *Mycobacterium* species such as *M. vanbaalenii* PYR-1, *M. smegmatis* MC2 155, *M. avium* sp. *paratuberculosis* and *M. kansasii* ATCC 12478 contain more than one CYP150 family member. In some species up to six genes encoding CYP150 family members can be found [23]. For example *M. vanbaalenii* PYR-1 has four, CYP150A7-10. As such, the CYP150 family appears prolific in *Mycobacterium* species, including human pathogens *M. ulcerans* and *M. colombiense* (Table S2). A BLAST search revealed there are a large number (~1000 entries with >55% identity) of similar proteins to both CYP150A5 and CYP150A6, the vast majority of which are from *Mycobacterium* (>90% of entries found). Enzymes of this family are also found in species of *Frankia*, *Streptomyces*, *Nocardia*, and *Rhodococcus* (see Table S2 for more details). This distribution of analogous enzymes in other Actinobacteria is similar to that observed for the *M. marinum* CYP enzymes CYP268A2 and CYP147G1 [26, 27, 47]. The analysis of Parvez *et al* placed the CYP150 family in a clan with the other *Mycobacterium* P450 families of CYP278, CYP1016, CYP269, CYP121, CYP1120, CYP1126, and CYP144 [23].

A sequence alignment of CYP150 family members (selected enzymes shown in Fig. S1) showed the proximal cysteine is conserved as Cys363 (the residue numbering is given for CYP150A6 which coincidentally is the same for CYP150A5) as is the nearby phenylalanine (Phe356). The EXXR motif is also conserved in all the CYP150 enzymes analysed (Fig. S1).

All contain an acid-alcohol pair; a glutamate (Glu255) and a threonine (Thr256). Phylogenetic analysis revealed CYP150A6 clusters closer to the previously studied *M. vanbaalenii* PYR-1 CYP150A7 (the polycyclic aromatic hydrolase [28]) and A8, while CYP150A9 and A10 are closer to CYP150A5 (Fig. 1). There appears to be two distinct CYP150 family groups; one containing CYP150A5 and the other with CYP150A6. However, all the CYP150 family members cluster together compared to the closest structurally characterised enzymes CYP144A1 from *M. tuberculosis* (32% identity to CYP150A5) and $P450_{BioI}$ from *Bacillus subtilis* (30% identity to CYP150A6).

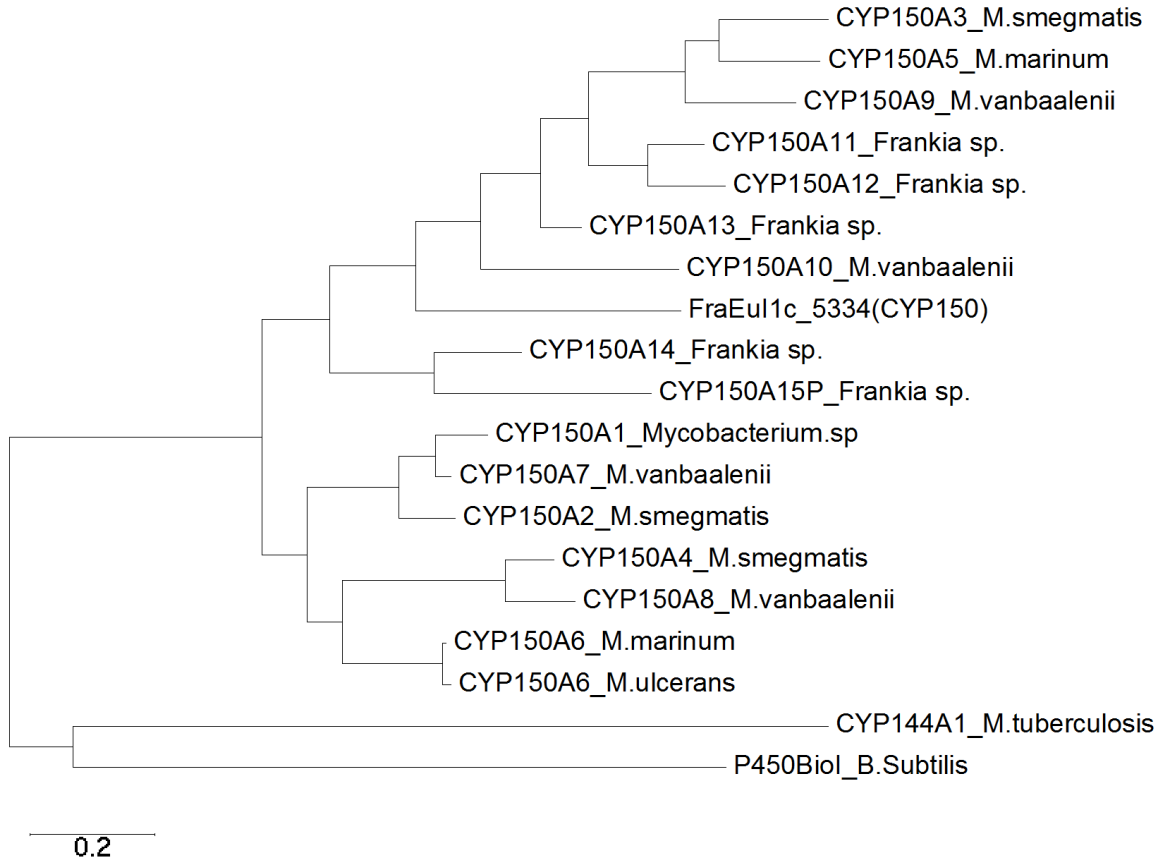

Figure 1: Phylogenetic tree (phenogram) of M. marinum enzymes CYP150A5 and CYP150A6 alongside other members of the CYP150 family from various *Mycobacterium* and other species. CYP150A7 from *M. vanbaalenii* has been reported to bind polyaromatic hydrocarbons. The CYP150 family member from *Frankia* sp. EuI1c (encoded by the gene *FraEuI1c_5334*) is included. The scale shows number of substitutions per site. CYP150A11, A12, A13 and A14 are from *Frankia* sp. EAN1pec.

The genomic context of the two CYP enzymes in *M. marinum* M is dissimilar (Fig. S2). CYP150A5 (*Mmar_4737)* lies near CYP190A3 (*Mmar*_4733) and there are three [3Fe-4S] ferredoxins nearby: *Mmar_4730*, *Mmar_4734* and *Mmar_4736*. *M. liflandii* 128FXT, *M. avium* sp. *paratuberculosis*, *M. smegmatis* MC2 155 and other *Mycobacterium* species show similar gene neighbours in the region of their CYP150A subfamily analogues. These also include a TetR transcriptional regular, an acyl-CoA dehydrogenase, an acyl-CoA acetyltransferase and an amidohydrolase. CYP150A9 from *M. vanbaalenii* PYR-1 has the most similar genomic region to that of CYP150A5 of the four CYP150 members from that species. In contrast, while CYP150A6 is present in *M. ulcerans* Agy99 (the sequence identity is 98%), comparison of the surrounding genomic region shows the enzyme is not part of a conserved operon. In *M. ulcerans* Agy99 CYP188A3 is nearby (three genes upstream) accompanied by a ferredoxin, while in *M. marinum* M the equivalent pair of genes are 23 genes downstream from CYP150A6. *Frankia* species that contain CYP150 family members show very little regional genomic similarity to *M. marinum* M (Fig. S2).

3.2 Characterisation of the CYP150 enzymes

The production, purification and quantitation of CYP150A5 has been reported previously in an investigation of the ferredoxin association with the CYPome of *M. marinum* [27]. CYP150A6 was produced recombinantly using *E. coli*, purified and the ferrous CO bound spectrum was recorded (mass confirmed by SDS-PAGE, Fig. S3). The absorbance of the enzyme's Soret peak shifts (>95%) to 450 nm upon reduction and CO exposure, indicating the reconstituted protein is a viable P450 enzyme (Fig. 2). The CYP150A6 enzyme demonstrated a comparable shift of the ferrous-CO bound form to CYP150A5 [27] and the extinction coefficient was determined to be ε_{418}=110 ± 6 mM^{-1} cm^{-1}.

In order to determine the substrate range, other members of the CYP150 family were considered. CYP150A7 from *M. vanbaalenii* has been reported to oxidise polyaromatic

hydrocarbons, such as pyrene, dibenzothiophene, and 7-methylbenz-α-anthracene [28]. However, as Brezna *et al* reported, there is no correlation between presence of a member of the CYP150 family and the polycyclic aromatic degradation ability of a particular strain, suggesting this may be a promiscuous activity of the enzyme [28].

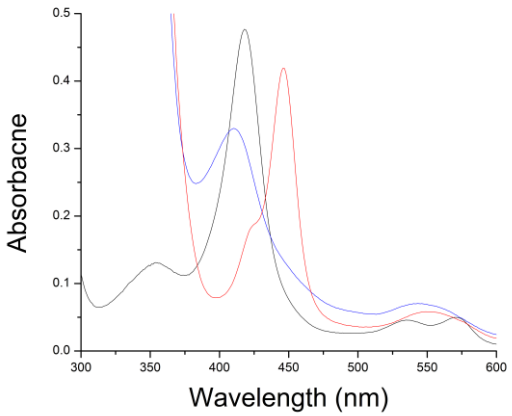

Figure 2: CYP150A6 (black, A418), the reduced ferrous (blue, A417) and the ferrous form bound with CO (red, A446) showing the characteristic ~450 nm absorbance. The shoulder at ~420 nm comprises < 5% of the total area. The extinction coefficient for the enzyme was determined to be $\varepsilon_{418} = 110 \pm 6$ mM^{-1} cm^{-1}.

The first substrates tested with both enzymes were therefore aromatic and polycyclic substrates. These included bicyclic aromatics such as naphthalene, naphthol, phenylphenol, tetralin, and quinoline. None perturbed the spin state of the CYP150A5 enzyme by more than 15% (see Table S3). Ionone derivatives such as α- and β-ionol, camphor and cineole as well as larger molecules such as sclareol and sclareolide were then assessed as substrates (Fig. 3). A large range of norisoprenoid substrates were capable of shifting the spin state shift of CYP150A5 to the high spin state (Table 2). These substrates included α-ionol (70% HS), methyl-α-ionone (65%), and α-ionone (45%). Interestingly, β-damascone, which differs in the location of the ketone group by only two carbons to the ionone substrates, shifted only 15% of the haem to the high spin form (compared to 60% high spin with β-ionone). (S)-(–)-Camphor (60%) and other monoterpenoid substrates such as bornyl acetate and isobornyl

acetate (75% and 70% respectively) also induced shifts indicative of a good substrate fit with the active site of the enzyme. The diterpene sclareol induced the highest spin state shift, at 90%, compared to 50% by sclareolide, which has an additional ring in the structure (Fig. 3). In contrast to the other hydrophobic aromatic compounds assessed, the bicyclic sesquiterpene guaiazulene shifted 60% of the haem to the high spin form. Both guaiazulene and 2-naphthol (70% high spin) were better substrates than 2-methylnapthalene (10%) suggesting the substituents around the aromatic ring are important to substrate recognition in CYP150A5.

Table 2: Substrate binding data for both CYP150A5 and CYP150A6. See Figure 4 for dissociation constant analysis. The Supplementary Information contains binding data of additional substrates (Table S3, Fig. S4 to S8).

Substrates	CYP150A5 Spin state shift (%)	K_D (μM)	CYP150A6 Spin state shift (%)
Sclareol	90	0.8 ± 0.08	10
Bornyl acetate	75	45 ± 6	10
Isobornyl acetate	70	34 ± 2	20
α-Ionol	70	17 ± 2	10
2-Naphthol	70	1900 ± 280	<5
Methyl-α-ionone	65	23 ± 4	10
Guaiazulene	60	1.9 ± 0.4	<5
β-Ionone	60	41 ± 2 [27]	15
1,8-Cineole	60	331 ± 45	<5
Fenchyl acetate	60	88 ± 13	10
β-Ionol	55	64 ± 6	20
Sclareolide	50	-	25

(-) indicates dissociation constant was not determined due to limitations in substrate solubility preventing the endpoint being reached.

Dissociation constant analyses were performed for compounds that, from the spin state shift, indicated they were complementary to the active site of CYP150A5 (defined here as where the shift to the high spin form was greater than 60%, Fig. 4). Sclareol had the highest binding affinity for the enzyme, at 0.8 ± 0.08 μM, followed by guaiazulene with 1.9 ± 0.4 μM. These were almost an order of magnitude higher than the next best, α-ionol (17 ± 2 μM). The previously reported affinity with β-ionone (41 ± 2 μM [27]) was similar to those

recorded for bornyl acetate (45 ± 6 µM) and slightly weaker than with isobornyl acetate (34 ± 2 µM). β-Ionol was less tightly bound (64 ± 6 µM). Despite the high spin state shifts recorded for naphthol and cineole with the enzyme, the dissociation constants indicated they bound weakly (1900 ± 280 µM and 331 ± 45 µM for 2-naphthol and 1,8-cineole, respectively). The results of this binding analysis provide evidence for a substrate range for CYP150A5 that includes both polycyclic hydrocarbons and terpenoid substrates.

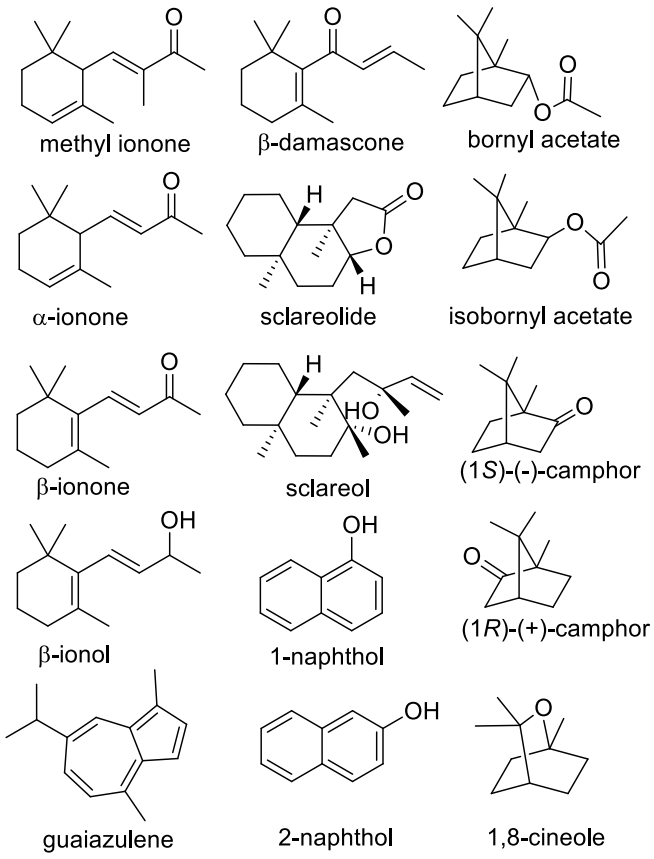

Figure 3: Structures of selected substrates tested with CYP150A5 and CYP150A6.

CYP150A6, in contrast, did not demonstrate any significant shifts in the spin state (all ≤ 25%) with any substrate tested. Sclareolide (25%), 1,4-cineole (20%), isobornyl acetate (20%) and β-ionol (20%) were the substrates that induced the greatest spin state shifts. A range of other substrates were tested, including fatty acids, benzoic acids, terpenoids, aromatics and steroids, however, no significant spin state shift was recorded (all ≤ 20%, Table S3 and Fig. S7). The CYP150A6 enzyme requires further characterisation as this

screening method did not reveal many substrates which were able to modify the spin state. This may suggest that the binding of the physiological substrate for this enzyme may be highly specific.

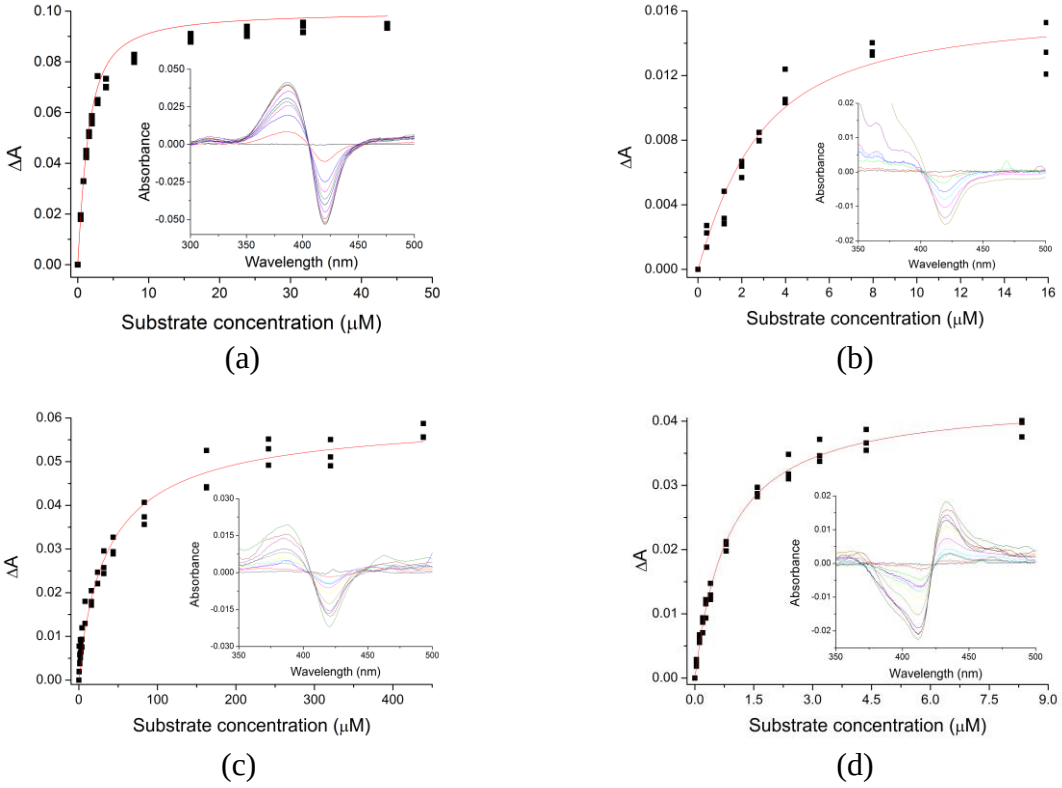

Figure 4: Dissociation constant analysis of CYP150A5 with (a) sclareol, (b) guaiazulene, (c) β-ionol and (d) ketoconazole. The inset represents a typical substrate titration. The peak to trough difference in absorbance was measured for (a) and (c), from 420 to 390 nm, for (b) trough to baseline (420 to 600 nm) due to interfering substrate absorbance and for (d) 432 to 411 nm. For additional dissociation constant analyses see Figure S5 and S6.

Both enzymes were tested with a range of azole compounds, known competitive inhibitors of CYPs (Fig. 5, Fig. S6 and Fig. S8). Econazole, ketoconazole and miconazole among others, generated Type II shifts in both enzymes indicative of N binding directly (or indirectly via a bridging H_2O ligand) to the haem Fe (Table 3). Both 1- and 4-phenylimidazole gave inhibitory shifts in both CYPs, while 2-phenylimidazole did not, similar to the results obtained with CYP268A2 and other P450 enzymes [26, 48, 49].

Fluconazole bound to CYP150A5, shifting the absorbance in a Type II manner, while with CYP150A6 a small (HS ~5%) Type I shift was observed suggesting it bound the enzyme in a substrate-like manner. In general, the phenylimidazoles bound less tightly, with dissociation constants in the tens of μM for both enzymes in contrast to the nanomolar affinities of the larger azoles.

Table 3: Binding data for possible inhibitors of both CYP150A5 and CYP150A6.

Possible inhibitors	**CYP150A5 Spin state shift**	**K_D (μM)**	**CYP150A6 Spin state shift**	**K_D (μM)**
1-Phenylimidazole	type II, 423 nm	19.2 ± 5.1	type II, 423 nm	29.9 ± 13.2
2-Phenylimidazole	~ 0%	-	~ 0%	-
Clotrimazole	type II, 424 nm	0.016 ± 0.01	type II, 425 nm	0.05 ± 0.02
Econazole	type II, 424 nm	0.01 ± 0.01	type II, 424 nm	1.1 ± 0.06
Fluconazole	type II, 419 nm	-	Type 1, ~5%	-
Ketoconazole	type II, 423 nm	0.80 ± 0.14	type II, 422 nm	6.6 ± 1
Miconazole	type II, 424 nm	0.045 ± 0.01	type II, 423 nm	1.0 ± 0.09

(-) indicates dissociation constant was not determined.

The affinity of the azoles were higher for CYP150A5 than CYP150A6 (for example, with econazole K_D = 0.01 ± 0.01 μM compared to 1.1 ± 0.06 μM for the respective enzymes). The affinity of clotrimazole for CYP150A6 was high in comparison to the other tested azoles with that enzyme (K_D = 0.05 ± 0.02 μM, two orders of magnitude tighter than the next best) although the CYP150A5 affinity (0.016 ± 0.01 μM) was greater still.

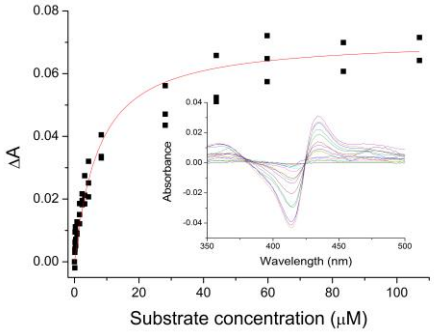

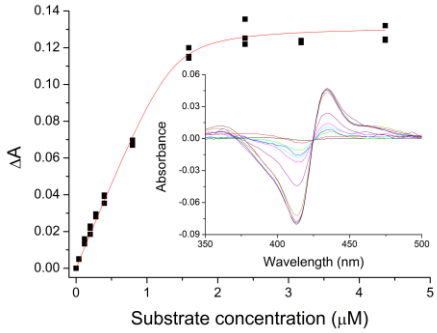

(a) (b)

Figure 5: Dissociation constants of CYP150A6 with (a) ketoconazole and (b) clotrimazole. The inset represents a typical substrate titration. The peak to trough difference in absorbance was measured from was (a) 435 to 414 nm and (b) 434 to 413 nm. For additional dissociations constants see Figure S8.

3.3 Product formation

Reconstitution of the *in vivo* activity of CYP150A5 was attempted with the native ferredoxin Fdx8 (*Mmar_4736*) as it is the adjacent gene to the CYP. No reductase gene is located nearby so the ferredoxin reductase FdR1 (*Mmar_2931*), which has been demonstrated to support CYP147G1 activity with Fdx3, was used [27]. Additional electron transfer systems including Tdx/ArR [7, 50], the fused phthalate dioxygenase reductase (PDR) domain from *Pseudomonas putida* pp_1957 [51], and other native ferredoxins from *M. marinum* were also tested (see Table S1). This included the ferredoxin seven genes away from CYP150A5, Fdx6 *(Mmar_4730)*. The product formation of each electron transfer system was tested with the substrate β-ionone. The native Fdx8 in combination with FdR1 was the best system tested.

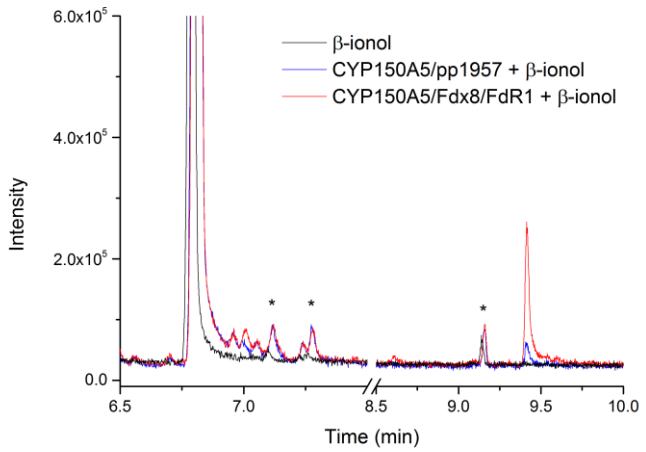

Figure 6: GC chromatogram of the *in vivo* turnover of CYP150A5 with Fdx8 and FdR1 (red) and the alternative electron transfer system of *pp*_1957 from *Pseudomonas putida* (blue) [51] both with the substrate β-ionol. β-Ionol (RT 6.9 min) converted into a single hydroxylation product, 4-hydroxy-β-ionol (RT 9.4 min). The physiological electron transfer partners Fdx8

and FdR1 supported greater CYP activity than the alternative systems tested, including *pp*_1957 (shown above, see Table S1 for others). * indicates a substrate impurity.

A range of substrates were tested with the CYP150A5 enzyme, including β-ionol and other terpenoids. A single hydroxylation product of β-ionol with CYP150A5 was visible by GC-MS analysis (Fig. 6). The mass spectrum and retention time corresponded to the 4-hydroxy-β-ionol product previously using CYP101B1 (Fig. S9)[52]. This is consistent with the 4-hydroxy product of β-ionone with the same enzyme. Again higher levels of metabolite formation were observed in combination with the Fdx8/FdR1 electron transfer partners (Fig. 6). However, product formation levels were still low and metabolites could not be detected with other substrates using the *in vivo* systems. Given the [3Fe-4S] Fdx8 ferredoxin is located nearby in the genome, the barrier to efficient electron transfer and oxidation may arise from the ferredoxin reductase. Further investigation into potential alternative reductases is required to optimise the system and to establish the full range of products that are generated.

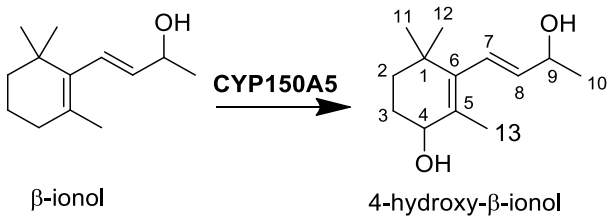

Scheme 1: CYP150A5 conversion of β-ionol to 4-hydroxy-β-ionol.

3.4 Crystal structure of CYP150A6

In order to better understand the substrate range of both enzymes we attempted crystallisation of both CYP150A5 and CYP150A6 in a range of conditions. No crystals were obtained for CYP150A5, but diffraction quality crystals were obtained for substrate-free CYP150A6. Data for CYP150A6 were collected from one crystal and the structure solved to 1.5 Å (Table 1, PDB: 6DCB). The structure presented difficulties in phasing that were resolved by using a truncated model of $P450_{BioI}$ prepared by Sculptor (as CYP150A6 lacks the acyl-carrier

domain of the $P450_{BioI}$ structure) [43]. Several regions required full rebuilding in Coot before refinement (residues 67 to 76 and 350 to 360). The final structure modelled the enzyme from residues 3 to 424 with the exception of the residues from 180 to 195 of the F-G loop for which the electron density was unresolved (Fig. 7). Despite the missing 16 residues, the overall structure of the enzyme clearly displays the conserved fold of a P450 with an open structure when compared to other structures in the PDB (composite omit map Fig. S10, and structural comparisons in Fig. S11 and S12). The disorder in the F-G loop is relatively common in previously characterised P450 enzymes in the open form [53, 54]. Both the F and G helices in CYP150A6 appear to be shorter than in most structurally characterised P450 isoforms (Fig. 7(b)), leaving a probable 18 residue long F-G loop region (in contrast *M. tuberculosis* CYP144A1 has only 3 residues between the F and G helices, Fig. S12). The proline residue at the end of the G helix (P199) is conserved in all *Mycobacterium* CYP150 members, while the glycine at the end of the F helix (G180) is conserved in *M. ulcerans* CYP150A6 and *M. vanbaalenii* CYP150A7, but not in CYP150A5 and some others, inferring that in these proteins the F helix may be longer. The length of the F and G helices is similar to those in mammalian CYP3A4, which has a large degree of substrate promiscuity [55, 56]. However the F-G loop region in CYP3A4 contains two further helices (F´ and G´) and is 35 residues long. As a result of the unresolved residues in CYP150A6, interpreting the precise nature of the active site and access channel is more challenging. As modelled, the active site appears to be very open to solvent (Fig. S13). The F and G helices may reform to a length similar to those in other systems when the enzyme is crystallised in the presence of a substrate.

The structure was compared to that of $P450_{BioI}$ (PDB: 3EJD), but the active site of the two structures present few similarities apart from the overall fold when overlaid (Fig. S12 and S15). An overlay with the closest structural model from *M. tuberculosis*, CYP144A1 (as

identified using MrBump and also the Dali server [57]) showed two regions of dissimilarity, including small α-helices (between the α-B and B′ region, and the other between α-L and β-5) that are not present in CYP144A1 [58]. These are referred to in this text as L′ and B″(Fig. 7(a)). The remaining best matches as identified by the Dali server were *Bacillus megaterium* CYP109A2 (PDB: 5OFQ)[59] and *M. tuberculosis* CYP142A1 (PDB: 2XKR). The β-sheet region in the B-C loop of CYP144A1 was absent in CYP150A6 (Fig. S11). The B-C loop area was more similar to that of the *M. smegmatis* CYP142A2 enzyme (PDB: 3ZBY, Fig. S12) [60].

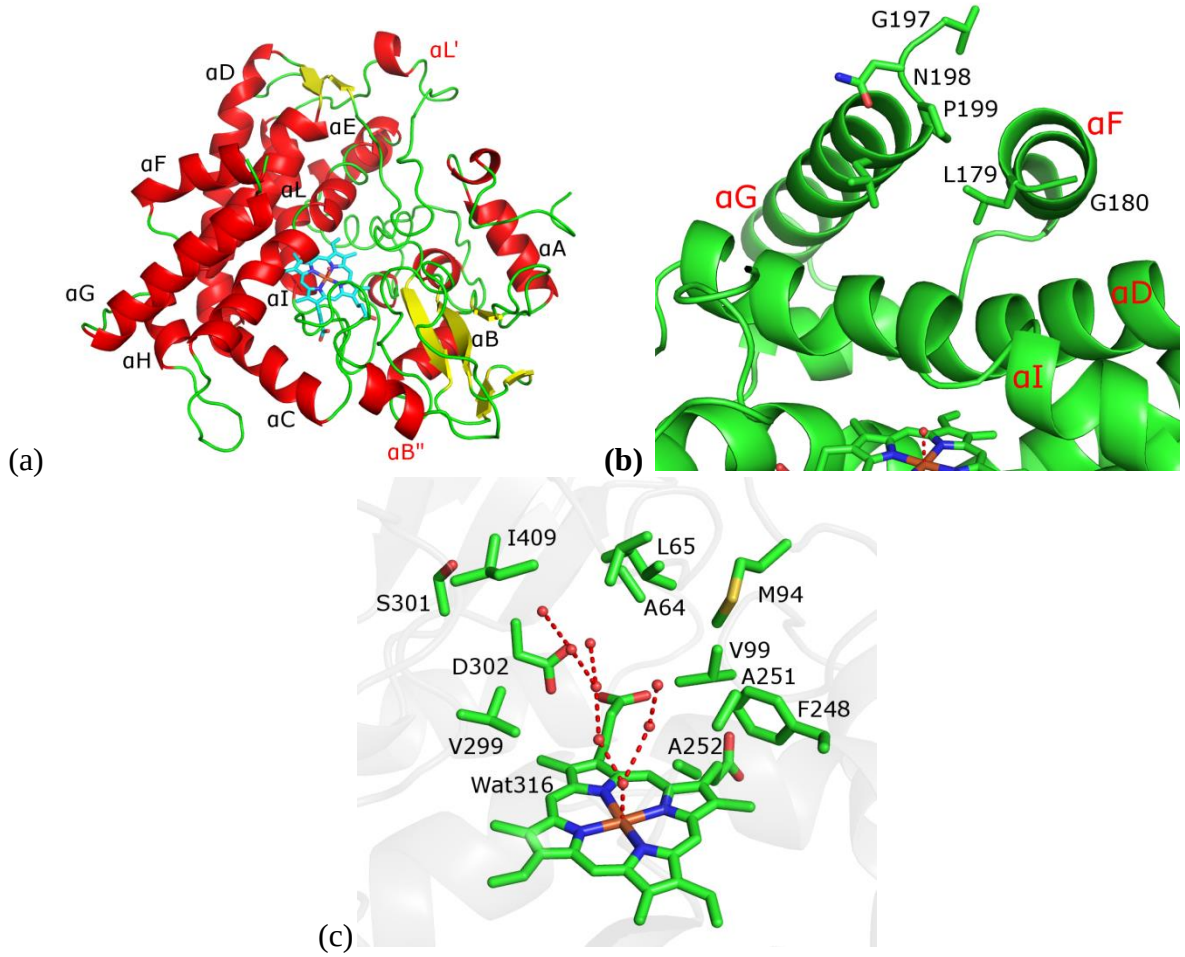

Figure 7: (a) CYP150A6 resolved to 1.5 Å with labelled α-helices according to the nomenclature developed in $P450_{cam}$ (CYP101A1) [61]. Helices are coloured in red, β-sheets in yellow and the remaining backbone in green. The haem is in blue. The two additional helices of CYP150A6 are labelled in red. In the absence of substrate a water molecule binds to the distal site of the haem Fe. (b) The key residues P199 and G180 at the end of the F and

G helices showing the short F and G loops (for comparison to other P450 structures see Figures S11 and S12). (c) The residues as well as the network of water molecules (hydrogen bonds in red) in the active site of the substrate-free CYP150A6 (green) enzyme.

The distal side of the haem contains an iron-bound water molecule (Wat316, Fe-O 2.2Å). Wat316 is stabilised by a network of hydrogen bonded waters in the active site (Fig. 7(c)). Two further water molecules (Wat110 and Wat10) are found bound in the kink of the I helix, forming hydrogen bonds between the A251 and T256 residues (where the T256 and E255 are the acid-alcohol pair of the enzyme, Fig. S14). The substrate binding pocket is primarily non-polar although the polar residues S301, D302 and M94 are present. The D302 residue, however, interacts with the carboxylate group of the haem (analogous to D297 in $P450_{cam}$ [62]). These, along with A64 and L65, V99, F248, A251 and A252, V299, and I409 can be identified as probable active site residues. The residues between 248 and 252 belong to the I helix (as seen in Fig. S14) while the B-C loop provides M94 and V99. As the residues of the F-G loop that may have formed the cap of the active site are not modelled, their probable interactions with a ligand cannot be seen. However, there is only limited evidence for direct substrate interaction with the F-G loop [63].

Applying the sequence alignment of CYP150A5 and other CYP150 enzymes to the structure of CYP150A6 allows the identification of the probable active site residues of those species (Table 4). The residues are very dissimilar between CYP150A6 and CYP150A5. Instead of the A251, CYP150A5 has a serine residue (the residue numbering in both enzymes is aligned so will not be given) while the S301 residue of CYP150A6 is changed to a glycine. F248 is changed to asparagine, while both the V99 and M94 residues are replaced with a phenylalanine. A64 and L65 are a serine and valine respectively in CYP150A5. Of the residues identified above, only the acid alcohol pair (E255 and T256), V299, D302 (which interacts with a haem carboxylate) and I409 are conserved in both enzymes. Together the changes would represent a significant alteration in the polarity and shape of the active site

between the enzymes, as reflected in the substrate binding results obtained for the two CYP isoforms.

Table 4: The active site residues of CYP150A6 and the aligned residues of other CYP150 family members, including CYP150A6 from *M. ulcerans*, CYP150A5 from *M. marinum* and all four enzymes from *M. vanbaalenii* PYR-1. Bold indicates the residue matches that of CYP150A6, underlined indicates it matches CYP150A5. For emphasis those that are conserved in all are given in red.[a] Additional CYP150 family members are listed in Table S4.

Mmar 150A6	**Mulc 150A6**	**Mmar 150A5**	**Msmeg 150A3**	**Mvan 150A7**	**Mvan 150A8**	**Mvan 150A9**	**Mvan 150A10**
A64	**A64**	S64	S65	**A64**	**A64**	S65	**A70**
L65	**L65**	V65	V66	**V65**	I65	V66	V71
M94	**M94**	F94	F96	**M94**	I94	F98	F100
V99	**V99**	P99	P101	**V99**	**V99**	P103	P105
F248	**F248**	N248	N250	**F253**	**F250**	N252	N253
A251	**A251**	S251	S253	**A256**	**A253**	S255	**A256**
A252	**A252**	**A252**	**A254**	**A257**	**A254**	**A256**	**A257**
V299	**V299**	**V299**	**V301**	**V304**	T301	**V303**	I304
I409	**I409**	**I409**	**I411**	**I414**	L411	**I413**	**I414**

[a] E255 and T256 (the acid alcohol pair) are also conserved in all but are not listed here.

The CYP150A6 enzyme in *M. ulcerans* Agy99 preserves all of the active site residues of the *M. marinum* equivalent, so it would be expected to both perform a similar function and the same inhibitors would be effective. Of the *M. vanbaalenii* PYR-1 enzymes, CYP150A7 has all the CYP150A6 active site residues conserved. CYP150A9 has equivalent residues to CYP150A5 at all these positions as does CYP150A3 from *M. smegmatis* MC2 155 (Table 4 and see Table S4 for other CYP150 family enzyme comparisons). The remaining two isoforms of *M. vanbaalenii* PYR-1, CYP150A8 and CYP150A10, share some active site residues with both *M. marinum* enzymes, and potentially would have distinct roles again.

4. Conclusions

Members of the CYP150 family are widely found in *Mycobacterium* species, as well as in related Actinomycetes. The only previously studied member of the family, CYP150A7 from *M. vanbaalenii* PYR-1, was found to oxidise certain polycyclic aromatic hydrocarbons which was linked to the activity of this species to degrade this class of compound. Here, the enzyme CYP150A5 is shown to bind and hydroxylate cyclic terpenes, with sclareol having the best binding parameters, rather than polycyclic aromatics. A physiological ferredoxin was used to support CYP activity in combination with a ferredoxin reductase also from *M. marinum.* The structural characterisation of CYP150A6 will facilitate future substrate identification for this enzyme through use of modelling and high-throughput screening methods. As both enzymes are found in a range of *Mycobacteria*, including human pathogens, the inhibitors which were determined for both enzymes could be used to stop CYP-related metabolism in these species which could form the basis of future drug design.

Acknowledgements

This work was supported by the Australian Research Council through a Future Fellowship (FT140100355 to S.G.B.). The authors also acknowledge the award of University of Adelaide Faculty of Sciences Divisional Scholarship (PhD to S.A.C.). X-ray diffraction data collection was undertaken on the MX1 beamline at the Australian Synchrotron, part of the Australian Nuclear Science and Technology Organisation (ANSTO). We acknowledge financial support from the Australian Synchrotron in the form of MXCAP9674. We are grateful to Professor Tim Stinear from the University of Melbourne and Professor Lalita Ramakrishnan of the University of Cambridge for providing the genomic DNA of *M. marinum.*

References

[1] P.R. Ortiz de Montellano, Substrate Oxidation by Cytochrome P450 Enzymes in: P.R. Ortiz de Montellano (Ed.) Cytochrome P450: Structure, Mechanism, and Biochemistry, Springer International Publishing, 2015, pp. 111-176.

[2] F.P. Guengerich, Common and uncommon cytochrome P450 reactions related to metabolism and chemical toxicity, Chem. Res. Tox, 14 (2001) 611-650.

[3] F. Hannemann, A. Bichet, K.M. Ewen, R. Bernhardt, Cytochrome P450 systems--biological variations of electron transport chains, Biochim. Biophys. Acta, 1770 (2007) 330-344.

[4] S.G. Bell, N. Hoskins, F. Xu, D. Caprotti, Z. Rao, L.L. Wong, Cytochrome P450 enzymes from the metabolically diverse bacterium *Rhodopseudomonas palustris*, Biochem. Biophys. Res. Commun., 342 (2006) 191-196.

[5] D.C. Lamb, T. Skaug, H.L. Song, C.J. Jackson, L.M. Podust, M.R. Waterman, D.B. Kell, D.E. Kelly, S.L. Kelly, The cytochrome P450 complement (CYPome) of *Streptomyces coelicolor* A3(2), J. Biol. Chem., 277 (2002) 24000-24005.

[6] D. Batabyal, T.L. Poulos, Crystal structures and functional characterization of wild-type CYP101D1 and its active site mutants, Biochemistry, 52 (2013) 8898-8906.

[7] S.G. Bell, A. Dale, N.H. Rees, L.-L. Wong, A cytochrome P450 class I electron transfer system from *Novosphingobium aromaticivorans*, Appl. Microbiol. Biotechnol., 86 (2010) 163-175.

[8] F.P. Guengerich, Human Cytochrome P450 Enzymes in: P.R. Ortiz de Montellano (Ed.) Cytochrome P450: Structure, Mechanism, and Biochemistry, Springer International Publishing, 2015, pp. 523-786.

[9] S.L. Kelly, D.E. Kelly, Microbial cytochromes P450: biodiversity and biotechnology. Where do cytochromes P450 come from, what do they do and what can they do for us?, Phil. Soc. Royal Soc. B, 368 (2013) 20120476.

[10] D.R. Nelson, L. Koymans, T. Kamataki, J.J. Stegeman, R. Feyereisen, D.J. Waxman, M.R. Waterman, O. Gotoh, M.J. Coon, R.W. Estabrook, I.C. Gunsalus, D.W. Nebert, P450 superfamily: update on new sequences, gene mapping, accession numbers and nomenclature, Pharmacogenetics, 6 (1996) 1-42.

[11] V.B. Urlacher, S. Eiben, Cytochrome P450 monooxygenases: perspectives for synthetic application, Trends in Biotechnol., 24 (2006) 324-330.

[12] World Health Organisation: Global Tuberculosis Report, in, http://www.who.int/tb/publications/global_report/en/, 2017.

[13] S.T. Cole, R. Brosch, J. Parkhill, T. Garnier, C. Churcher, D. Harris, S.V. Gordon, K. Eiglmeier, S. Gas, C.E. Barry, 3rd, F. Tekaia, K. Badcock, D. Basham, D. Brown, T. Chillingworth, R. Connor, R. Davies, K. Devlin, T. Feltwell, S. Gentles, N. Hamlin, S. Holroyd, T. Hornsby, K. Jagels, A. Krogh, J. McLean, S. Moule, L. Murphy, K. Oliver, J. Osborne, M.A. Quail, M.A. Rajandream, J. Rogers, S. Rutter, K. Seeger, J. Skelton, R. Squares, S. Squares, J.E. Sulston, K. Taylor, S. Whitehead, B.G. Barrell, Deciphering the biology of *Mycobacterium tuberculosis* from the complete genome sequence, Nature, 393 (1998) 537-544.

[14] K.J. McLean, A.J. Dunford, R. Neeli, M.D. Driscoll, A.W. Munro, Structure, function and drug targeting in *Mycobacterium tuberculosis* cytochrome P450 systems, Arch. Biochem. Biophys., 464 (2007) 228-240.

[15] H. Ouellet, J.B. Johnston, P.R. Ortiz de Montellano, The *Mycobacterium tuberculosis* cytochrome P450 system, Arch. Biochem. Biophys., 493 (2010) 82-95.

[16] K.J. McLean, P. Carroll, D.G. Lewis, A.J. Dunford, H.E. Seward, R. Neeli, M.R. Cheesman, L. Marsollier, P. Douglas, W.E. Smith, I. Rosenkrands, S.T. Cole, D. Leys, T. Parish, A.W. Munro, Characterization of active site structure in CYP121. A cytochrome P450 essential for viability of *Mycobacterium tuberculosis* H37Rv, J. Biol. Chem., 283 (2008) 33406-33416.

[17] P. Belin, M.H. Le Du, A. Fielding, O. Lequin, M. Jacquet, J.B. Charbonnier, A. Lecoq, R. Thai, M. Courcon, C. Masson, C. Dugave, R. Genet, J.L. Pernodet, M. Gondry, Identification and structural basis of the reaction catalyzed by CYP121, an essential cytochrome P450 in *Mycobacterium tuberculosis*, Proc. Nat. Acad. Sci. U.S.A, 106 (2009) 7426-7431.

[18] S.A. Hudson, K.J. McLean, S. Surade, Y.Q. Yang, D. Leys, A. Ciulli, A.W. Munro, C. Abell, Application of Fragment Screening and Merging to the Discovery of Inhibitors of the *Mycobacterium tuberculosis* Cytochrome P450 CYP121, Angew. Chem. Int. Ed., 51 (2012) 9311-9316.
[19] K.M. Sogi, C.M. Holsclaw, G.K. Fragiadakis, D.K. Nomura, J.A. Leary, C.R. Bertozzi, Biosynthesis and regulation of sulfomenaquinone, a metabolite associated with virulence in *Mycobacterium tuberculosis*, ACS Infect. Dis., 2 (2016) 800-806.
[20] J.K. Capyk, R. Kalscheuer, G.R. Stewart, J. Liu, H. Kwon, R. Zhao, S. Okamoto, W.R. Jacobs, Jr., L.D. Eltis, W.W. Mohn, Mycobacterial cytochrome p450 125 (*cyp125*) catalyzes the terminal hydroxylation of c27 steroids, J. Biol. Chem., 284 (2009) 35534-35542.
[21] M.D. Driscoll, K.J. McLean, C. Levy, N. Mast, I.A. Pikuleva, P. Lafite, S.E. Rigby, D. Leys, A.W. Munro, Structural and biochemical characterization of *Mycobacterium tuberculosis* CYP142: evidence for multiple cholesterol 27-hydroxylase activities in a human pathogen, J. Biol. Chem., 285 (2010) 38270-38282.
[22] D.A. Stahl, J.W. Urbance, The division between fast- and slow-growing species corresponds to natural relationships among the mycobacteria, J. Bacteriol., 172 (1990) 116-124.
[23] M. Parvez, L.B. Qhanya, N.T. Mthakathi, I.K.R. Kgosiemang, H.D. Bamal, N.S. Pagadala, T. Xie, H. Yang, H. Chen, C.W. Theron, R. Monyaki, S.C. Raselemane, V. Salewe, B.L. Mongale, R.G. Matowane, S.M.H. Abdalla, W.I. Booi, M. van Wyk, D. Olivier, C.E. Boucher, D.R. Nelson, J.A. Tuszynski, J.M. Blackburn, J.-H. Yu, S.S. Mashele, W. Chen, K. Syed, Molecular evolutionary dynamics of cytochrome P450 monooxygenases across kingdoms: Special focus on mycobacterial P450s, Sci. Rep., 6 (2016) 33099.
[24] C. Demangel, T.P. Stinear, S.T. Cole, Buruli ulcer: reductive evolution enhances pathogenicity of *Mycobacterium ulcerans*, Nature Reviews. Microbiol., 7 (2009) 50-60.
[25] T.P. Stinear, T. Seemann, P.F. Harrison, G.A. Jenkin, J.K. Davies, P.D. Johnson, Z. Abdellah, C. Arrowsmith, T. Chillingworth, C. Churcher, K. Clarke, A. Cronin, P. Davis, I. Goodhead, N. Holroyd, K. Jagels, A. Lord, S. Moule, K. Mungall, H. Norbertczak, M.A. Quail, E. Rabbinowitsch, D. Walker, B. White, S. Whitehead, P.L. Small, R. Brosch, L. Ramakrishnan, M.A. Fischbach, J. Parkhill, S.T. Cole, Insights from the complete genome sequence of *Mycobacterium marinum* on the evolution of *Mycobacterium tuberculosis*, Genome Res., 18 (2008) 729-741.
[26] S.A. Child, E.F. Naumann, J.B. Bruning, S.G. Bell, Structural and functional characterisation of the cytochrome P450 enzyme CYP268A2 from *Mycobacterium marinum*, Biochem. J., 475 (2018) 705-722.
[27] S.A. Child, J.M. Bradley, T.L. Pukala, D.A. Svistunenko, N.E. Le Brun, S.G. Bell, Electron transfer ferredoxins with unusual cluster binding motifs support secondary metabolism in *Mycobacteria* and are prevalent in many other bacteria, Chem. Sci., 9 (2018) 7948-7957.
[28] B. Brezna, O. Kweon, R.L. Stingley, J.P. Freeman, A.A. Khan, B. Polek, R.C. Jones, C.E. Cerniglia, Molecular characterization of cytochrome P450 genes in the polycyclic aromatic hydrocarbon degrading *Mycobacterium vanbaalenii* PYR-1, Appl. Microbiol. Biotechnol., 71 (2006) 522-532.
[29] J. Sambrook, T. Maniatis, E.F. Fritsch, Molecular cloning : a laboratory manual, Cold Spring Harbor Laboratory Press, 1987.
[30] T. Omura, R. Sato, The Carbon Monoxide-Binding Pigment of Liver Microsomes. Ii. Solubilization, Purification, and Properties, J. Biol. Chem., 239 (1964) 2379-2385.
[31] J.M. Dogne, X. de Leval, P. Benoit, S. Rolin, B. Pirotte, B. Masereel, Therapeutic potential of thromboxane inhibitors in asthma, Expert Opin. Investig. Drugs, 11 (2002) 275-281.
[32] D.R. Nelson, The cytochrome p450 homepage, Hum. Genomics, 4 (2009) 59-65.
[33] F. Sievers, A. Wilm, D. Dineen, T.J. Gibson, K. Karplus, W. Li, R. Lopez, H. McWilliam, M. Remmert, J. Soding, J.D. Thompson, D.G. Higgins, Fast, scalable generation of high-quality protein multiple sequence alignments using Clustal Omega, Mol. Syst. Bio., 7 (2011) 539.
[34] D.T. Jones, W.R. Taylor, J.M. Thornton, The rapid generation of mutation data matrices from protein sequences, Comput. Appl. Biosci.,8 (1992) 275-282.
[35] K. Tamura, G. Stecher, D. Peterson, A. Filipski, S. Kumar, MEGA6: Molecular Evolutionary Genetics Analysis version 6.0, Mol. Biol. Evol., 30 (2013) 2725-2729.
[36] T.M. McPhillips, S.E. McPhillips, H.J. Chiu, A.E. Cohen, A.M. Deacon, P.J. Ellis, E. Garman, A. Gonzalez, N.K. Sauter, R.P. Phizackerley, S.M. Soltis, P. Kuhn, Blu-Ice and the Distributed

Control System: software for data acquisition and instrument control at macromolecular crystallography beamlines, J. Synchrotron Radiat., 9 (2002) 401-406.
[37] T.G. Battye, L. Kontogiannis, O. Johnson, H.R. Powell, A.G. Leslie, iMOSFLM: a new graphical interface for diffraction-image processing with MOSFLM, Acta. Crystallog. D, 67 (2011) 271-281.
[38] P.R. Evans, G.N. Murshudov, How good are my data and what is the resolution?, Acta. Crystallog. D, 69 (2013) 1204-1214.
[39] M.D. Winn, C.C. Ballard, K.D. Cowtan, E.J. Dodson, P. Emsley, P.R. Evans, R.M. Keegan, E.B. Krissinel, A.G. Leslie, A. McCoy, S.J. McNicholas, G.N. Murshudov, N.S. Pannu, E.A. Potterton, H.R. Powell, R.J. Read, A. Vagin, K.S. Wilson, Overview of the CCP4 suite and current developments, Acta. Crystallog. D, 67 (2011) 235-242.
[40] R.M. Keegan, M.D. Winn, Automated search-model discovery and preparation for structure solution by molecular replacement, Acta Crystallog. D, 63 (2007) 447-457.
[41] A.J. McCoy, R.W. Grosse-Kunstleve, P.D. Adams, M.D. Winn, L.C. Storoni, R.J. Read, Phaser crystallographic software, J. Appl. Crystallog., 40 (2007) 658-674.
[42] K. Cowtan, The Buccaneer software for automated model building. 1. Tracing protein chains, Acta. Crystallog. D, 62 (2006) 1002-1011.
[43] M.J. Cryle, I. Schlichting, Structural insights from a P450 Carrier Protein complex reveal how specificity is achieved in the P450(BioI) ACP complex, Proc. Nat. Acad. Sci. U.S.A, 105 (2008) 15696-15701.
[44] A. Vagin, A. Teplyakov, MOLREP: an Automated Program for Molecular Replacement, J. Appl. Crystallog., 30 (1997) 1022-1025.
[45] P. Emsley, B. Lohkamp, W.G. Scott, K. Cowtan, Features and development of Coot, Acta. Crystallog. D, 66 (2010) 486-501.
[46] P.D. Adams, P.V. Afonine, G. Bunkoczi, V.B. Chen, I.W. Davis, N. Echols, J.J. Headd, L.W. Hung, G.J. Kapral, R.W. Grosse-Kunstleve, A.J. McCoy, N.W. Moriarty, R. Oeffner, R.J. Read, D.C. Richardson, J.S. Richardson, T.C. Terwilliger, P.H. Zwart, PHENIX: a comprehensive Python-based system for macromolecular structure solution, Acta. Crystallog. D, 66 (2010) 213-221.
[47] S.A. Child, V.P. Rossi, S.G. Bell, Selective ω-1 oxidation of fatty acids by CYP147G1 from *Mycobacterium marinum*, Biochim. Biophys. Acta. Gen. Subj., 1863 (2019) 408-417.
[48] K.J. McLean, A.J. Warman, H.E. Seward, K.R. Marshall, H.M. Girvan, M.R. Cheesman, M.R. Waterman, A.W. Munro, Biophysical characterization of the sterol demethylase P450 from *Mycobacterium tuberculosis*, its cognate ferredoxin, and their interactions, Biochemistry, 45 (2006) 8427-8443.
[49] D.L. Harris, Y.-T. Chang, G.H. Loew, Molecular dynamics simulations of phenylimidazole inhibitor complexes of cytochrome P450 cam, Molec. Eng., 5 (1995) 143-156.
[50] S.G. Bell, W. Yang, J.A. Yorke, W. Zhou, H. Wang, J. Harmer, R. Copley, A. Zhang, R. Zhou, M. Bartlam, Z. Rao, L.L. Wong, Structure and function of CYP108D1 from *Novosphingobium aromaticivorans* DSM12444: an aromatic hydrocarbon-binding P450 enzyme, Acta. Crystallog. D, 68 (2012) 277-291.
[51] S.G. Bell, L. French, N.H. Rees, S.S. Cheng, G. Preston, L.L. Wong, A phthalate family oxygenase reductase supports terpene alcohol oxidation by CYP238A1 from *Pseudomonas putida* KT2440, Biotechnol. Appl. Biochem., 60 (2013) 9-17.
[52] E.A. Hall, M.R. Sarkar, J.H.Z. Lee, S.D. Munday, S.G. Bell, Improving the Monooxygenase Activity and the Regio- and Stereoselectivity of Terpenoid Hydroxylation Using Ester Directing Groups, ACS Catal., 6 (2016) 6306-6317.
[53] T.L. Poulos, Cytochrome P450 flexibility, Proc. Nat. Acad. Sci. U.S.A, 100 (2003) 13121-13122.
[54] T.C. Pochapsky, S. Kazanis, M. Dang, Conformational Plasticity and Structure/Function Relationships in Cytochromes P450, Antiox. Redox Signaling, 13 (2010) 1273-1296.
[55] J.K. Yano, M.R. Wester, G.A. Schoch, K.J. Griffin, C.D. Stout, E.F. Johnson, The Structure of Human Microsomal Cytochrome P450 3A4 Determined by X-ray Crystallography to 2.05-Å Resolution, J. Biol. Chem, 279 (2004) 38091-38094.
[56] P.A. Williams, J. Cosme, D.M. Vinković, A. Ward, H.C. Angove, P.J. Day, C. Vonrhein, I.J. Tickle, H. Jhoti, Crystal Structures of Human Cytochrome P450 3A4 Bound to Metyrapone and Progesterone, Science, 305 (2004) 683-686.
[57] L. Holm, L.M. Laakso, Dali server update, Nucleic Acids Res, 44 (2016) W351-355.

[58] J. Chenge, M.E. Kavanagh, M.D. Driscoll, K.J. McLean, D.B. Young, T. Cortes, D. Matak-Vinkovic, C.W. Levy, S.E. Rigby, D. Leys, C. Abell, A.W. Munro, Structural characterization of CYP144A1 - a cytochrome P450 enzyme expressed from alternative transcripts in *Mycobacterium tuberculosis*, Sci. Rep., 6 (2016) 26628.
[59] A. Abdulmughni, I.K. Jozwik, E. Brill, F. Hannemann, A.W.H. Thunnissen, R. Bernhardt, Biochemical and structural characterization of CYP109A2, a vitamin D3 25-hydroxylase from *Bacillus megaterium*, FEBS J., 284 (2017) 3881-3894.
[60] E. Garcia-Fernandez, D.J. Frank, B. Galan, P.M. Kells, L.M. Podust, J.L. Garcia, P.R. Ortiz de Montellano, A highly conserved mycobacterial cholesterol catabolic pathway, Environ. Microbiol., 15 (2013) 2342-2359.
[61] T.L. Poulos, B.C. Finzel, I.C. Gunsalus, G.C. Wagner, J. Kraut, The 2.6-A crystal structure of *Pseudomonas putida* cytochrome P-450, J. Biol. Chem., 260 (1985) 16122-16130.
[62] T.L. Poulos, B.C. Finzel, A.J. Howard, High-resolution crystal structure of cytochrome P450cam, J. Mol. Bio., 195 (1987) 687-700.
[63] S.C. Dodani, G. Kiss, J.K.B. Cahn, Y. Su, V.S. Pande, F.H. Arnold, Discovery of a regioselectivity switch in nitrating P450s guided by molecular dynamics simulations and Markov models, Nat. Chem., 8 (2016) 419.